Journal of Cultural Heritage 68 (2024) 28–37

Contents lists available at ScienceDirect

Journal of Cultural Heritage

journal homepage: www.elsevier.com/locate/culher

Original article

Potential of synchrotron X-ray diffraction computed tomography (XRDCT) for a 3D non-destructive and/or non-invasive characterisation of cultural heritage geomaterials (CHG)

Elena Possenti [a,*], Maria Catrambone [a], Chiara Colombo [a], Marco Cantaluppi [b], Marco Merlini [b], Gavin B.M. Vaughan [c], Marco di Michiel [c], Nicoletta Marinoni [b,*]

[a] Institute of Heritage Science, National Research Council, ISPC-CNR, Via R. Cozzi 53, 20125 Milan, Italy
[b] Department of Earth Sciences "Ardito Desio", University of Milan, Italy, Via Botticelli 23, 20133 Milan, Italy
[c] European Synchrotron Radiation Facility, BP 220, 38043 Grenoble, France

ARTICLE INFO

Article history:
Received 17 January 2024
Accepted 10 April 2024

Keywords:
Synchrotron radiation X-ray diffraction computed tomography (XRDCT)
Geomaterials of cultural heritage
Archaeological ceramics
Inorganic-mineral conservation treatment
Stone materials of built Heritage
Meteorites

ABSTRACT

The present work describes the high potential of the recently developed synchrotron X-ray diffraction computed tomography (XRDCT) for 3D mapping of crystalline and amorphous phases in Geomaterials of Cultural Heritage (CHG). The paper critically discusses the promising results and limitations of XRDCT in Cultural Heritage applications. XRDCT has been applied herein to diverse CHG materials, spanning from archaeological ceramics, and stone conservation treatments to meteorites, at a microscale. Although these materials are very complex systems from a chemical, mineralogical and microstructural point of view, this innovative technique proves effective capability to access the real spatial distribution and semi-quantification of crystallographic phases within materials in a totally non-destructive and/or non-invasive way.

1. Introduction and research aim

The term Cultural Heritage Geomaterials (CHG) is here introduced to comprise natural rocks and rock-like materials such as mortar, concrete, painting, ceramic, etc. which belong to a wide range of scientific fields from Geology, Conservation Science, Archaeometry, among others, and constitute an open window on Cultural Heritage (CH) and humankind's past. Understanding the microstructure of CHG is important for interpreting their evolution in time from the raw materials, through the man-made production and transformation processes, their use, spread throughout the world, and for estimating their degradation state which is crucial for conservation.

In the last decade, a multidisciplinary approach has been applied to the study of CHG, using different experiences and skills necessary to achieve a common objective. This has allowed us to obtain better documentation of the CHG and its conservation state. Collecting simultaneously their chemical, mineralogical and morphological information is fundamental for developing new preservation and conservation strategies. Several important studies of CHG have been made based on 2D imaging techniques utilising polarisation optical microscopy and scanning electron microscopy. However, these techniques require destructive sample preparation, which is not trivial for CHG because (i) a non-destructive and/or non-invasive approach is preferred, especially in CH and (ii) the preparation can cause massive modification to the sample under study. For instance, embedding in synthetic resin, cutting and polishing as well as sample drying in vacuum-dependent techniques may significantly and irreversibly change the material's original morphology. In this study, "non-destructive" refers to analytical methods that involve the sampling of a micro-fragment from a CH object but that do not alter its chemical and physical state, and do not require any sample preparation. Conversely, "non-invasive" comprises analytical techniques able to investigate whole objects without the need of any sampling.

X-ray diffraction (XRD) has been extensively used in material sciences to identify and quantify crystalline/amorphous compounds even in complex polyphasic mixtures [1,2]. However, the

* Corresponding authors.
E-mail addresses: elena.possenti@cnr.it (E. Possenti), nicoletta.marinoni@unimi.it (N. Marinoni).

https://doi.org/10.1016/j.culher.2024.04.006

most limiting factor in the experimental measurement of CHG materials is commonly derived from the scarcity of available samples (if any). To avoid any sampling, XRD investigations could be carried out non-invasively with portable XRD instruments or by bringing movable CH artefacts to XRD fix labs [3–5]. In this latter case, the technique generally requires an instrumental setup (i.e. very energetic beam to investigate the bulk) that can be found at large-scale facilities, especially synchrotron X-ray and neutron sources.

Additionally, XRD mapping has become relevant in the investigation of CHG: it consists of acquiring XRD patterns at each pixel of a two-dimensional (2D) area either at the macro or micro scale. In mapping mode the information extracted from XRD patterns (mineralogy, phase orientation, texture, etc.) can be combined with spatial information and two-dimensional distribution maps of these features can be composed. This technique is currently applied in the field of CH, mainly in the characterisation of painting, ceramics, manuscripts, concrete, etc. [6–8]. On the other hand, such an XRD approach requires that CHG are prepared as transversal (thin) cross-sections compatible (in terms of sample dimension, composition, and density in the direction perpendicular to the cross-section surface) for sufficient transmission of X-rays at a given energy [9].

Moreover, the CH objects are often multi-layered systems of micrometric thickness (i.e. paintings) and/or are very complex polyphasic composites (i.e. mortars, ceramics, etc.) and the complex build-up and spatial arrangement of these materials in 3D is therefore important. Consequently, there is a need for non-destructive and non-invasive 3D techniques capable of investigating CHG to reveal chemical and mineralogical information at high resolution across a wide 3D field of view. Recent advances include 3D imaging which is regularly employed to identify and map materials from the nano to macroscale. Conventional attenuation and phase-contrast X-ray Computed Tomography (CT) enables us to image the internal structure of an object/sample, investigating the morphological features and the topography of different phases (solid phases and/or voids) [10–16]. However, CT is strongly limited when it comes to distinguishing materials of low-density contrast (i.e. phases with a similar chemical composition) and does not supply any crystallo-chemical information about the material phases.

CT analysis and XRD signals can be combined allowing the 3D imaging of the materials where the crystalline and/or amorphous phases are used as contrast mechanisms, thus allowing materials with similar density to be distinguished. This innovative technique is called X-ray diffraction Computed Tomography (XRDCT) and combines the high selectivity of XRD techniques for crystalline phases with the 3D imaging potentialities of CT. Therefore, XRDCT can be used to map the spatial distribution of selected crystalline (or amorphous) phases within a given sample, offering a powerful chemical imaging method for the investigation of a wide range of heterogeneous materials with a non-invasive approach [15,17,18].

Recently, XRDCT has been gaining increasing attention and recent studies reported outstanding results in different areas of material sciences, such as the field of heterogeneous catalysis, of the cement industry [17–23] and it is still a niche analytical approach not widely exploited in the characterisation of unique geomaterials of Cultural Heritage [24–26]. XRDCT is generally applied at synchrotron facilities as it requires an experimental setup with a micrometric, collimated, and energetic hard X-ray beam and with a high brilliance. At present, several beamlines at different synchrotron facilities offer today the possibility to perform XRDCT (e.g., beamlines at DESY, ESRF, Spring8). However, the processing of XRDCT data is so challenging that, notwithstanding its high potential, this technique has a limited use.

The study aims to demonstrate the feasibility and high potential of the XRDCT technique to reconstruct, in a totally non-destructive and/or non-invasive way, the 3D distribution of the crystalline and/or amorphous phases in CHG. In this paper, XRDCT is applied to different CH geomaterials with heterogeneous characteristics in chemical and mineralogical composition scaled down to the microscale. In particular, the present research focuses on (i) a Roman pottery from the Nile Valley which represents an artificial material obtained by firing a clay-based paste, (ii) an inorganic-mineral conservation treatment applied to consolidate stone materials of built heritage, and (iii) a meteorite from the collection of the Mineralogical Museum of the University of Milan as an example of geological material of extraterrestrial origin. Finally, the potential and limitations of the XRDCT technique in the field of Cultural Heritage are critically discussed.

2. Materials

The CHG samples selected for the present study exhibit a high complexity due to (i) intrinsic and (ii) extrinsic factors. In particular, the formers are mainly attributed to the object/sample itself, as many of the CH objects are multiphase and heterogeneous systems with different origins (terrestrial/extra-terrestrial materials; natural/artificial materials) and with complex chemistry (alloys/solid solutions), mineralogy (mixture of different crystalline phases; polymorphs; co-existence of crystalline/amorphous phases) and microstructure (systems composed by crystals of different grain size). The latter is linked to the CH fields, as the need to obtain the maximum amount of structural and volume information on the materials avoiding (or with the minimum) damages/alteration on the investigated sample/object poses significant analytical challenges.

Case study #1: Roman ancient pottery from Nile Valley

Personnel from the University of Milan participated in an archaeological mission from 1990 to 1996, which aimed to study the life and material culture in the TadrartAcacus and surrounding areas. The mission collected a significant amount of pottery samples, including the *ARA13-2* sample, which is part of a collection of ceramics dating back to the Roman period and originating from the Nile valley, particularly from Sudan and Egypt.

Note that no sample handling (i.e. cutting, polishing, etc.) is required for the XRDCT investigation, so the ancient pottery has been analysed as it stands. This case study aims to be an example of a non-invasive approach to the characterisation of CHG.

Case study #2: Consolidation of calcareous stone materials with a phosphate-based conservation treatment

The Angera stone, a porous, sedimentary Triassic dolostone mainly composed of dolomite ($CaMg(CO_3)_2$) has been used for the study. This lithotype is quarried in Northern Italy (Piedmont) in three peculiar colour shades, namely pink, white, and pale ochre, according to the presence of iron oxides and clay impurities [27]. It has been widely used as a building material in Lombard architecture since the Roman age due to its typical colour variations giving rise to ornamental decorative patterns [28,29]. Diagnostic studies aimed to conserve works in the San Fedele church and the Cortile del Richini (Milan), a masterpiece of the Lombard Baroque in Milan.

The white Angera stone shows a microcrystalline texture with stone grains weakly bonded to each other, which leads to peculiar decay phenomena when carved artefacts are exposed to polluted environments. Hence, the white variety of Angera stone was selected for the investigations. In recent years, a more compatible conservation approach based on diammonium hydrogen phosphate (DAP, $(NH_4)_2HPO_4$)) inorganic-mineral treatments has been proposed to consolidate decayed dolostones and DAP solutions have been applied to the Angera stone for the first time [30]. In this study, the Angera stone specimens ($50 \times 50 \times 20$ mm^3) were consolidated by poultice (dry cellulose pulp, MH 300 Phase, Italy; ratio

~ 5:1 DAP solution:dry cellulose pulp) with a 0.76 M aqueous solution of DAP [31].

Suitable samples for XRDCT measurements (cylinders with diameter 1.5–1.0 mm) were obtained by cutting the 50 × 50 × 20 mm^3 specimens after the DAP treatment to explore the crystallisation and volume distribution of the novel phosphate phases formed from DAP solutions at room temperature within dolostones. This case study would serve as an example of a non-destructive approach in the characterisation of CHG.

Case study #3: Meteorite

The analysed meteorite fragment originates from the Holbrook meteorite, Arizona, and is classified as a chondrite. From a mineralogical point of view, it is predominantly composed of olivine, pyroxene, plagioclase, iron-nickel alloy, and troilite [32]. This millimetric fragment is stored in the collections of the "Museo delle collezioni mineralogiche, gemmologiche, petrografiche e giacimentologiche" of the University of Milan, alongside a larger fragment and other smaller fragments. As for *Case study #1* note that no sample handling (i.e., cutting, polishing, etc.) is required for the XRDCT investigation. This case study would be an example of a non-invasive approach to the characterisation of CHG.

3. Methods

3.1. Optical microscopy

Thin sections were studied under a Leitz polarised light microscope connected to a 51 MP camera, using magnifications 2.5 and 10X.

3.2. X-Ray powder diffraction analysis (XRPD) and Rietveld Method

XRPD data acquisition was carried out by a X'Pert PRO Diffractometer (PANalytical), in $\theta-2\theta$ Bragg-Brentano geometry with a diverging beam diffractometer, equipped with an X'Celerator LPS detector. The 1.23–7.75 d (Å) range has been investigated using CuKα radiation for all samples. All XRPD analyses were performed with a 40 kV/40 mA current and a 0.02° step size. The equivalent counting time was 120 s/step for all the samples, with a fixed divergence slit angle of 0.5°.

XRPD profiles were fit using the GSAS-II software for quantitative analysis by means of the Rietveld Method. The instrumental calibration of the laboratory diffractometer was performed by analysing LaB_6 (SRM 660c) in the same experimental setups, thus obtaining the instrumental profile parameters (U, V, W, X, Y and SH/L) needed for quantitative analysis by the Rietveld Method. In particular, cell parameters, crystallite size, individual scale factors, zero shift, and a Chebychev polynomial function used to model the background functions were refined during Rietveld analysis.

3.3. External reflection (ER) Fourier transform infrared (FTIR) spectroscopy

The ER-FTIR measurements were carried out with an Alpha II spectrometer (Bruker Optics, Germany) equipped with an external reflection module. The spectra were acquired in the near- and mid-infrared region from 8000 to 400 cm^{-1}, at a resolution of 4 cm^{-1} by collecting 128 scans. The ER-FTIR investigations were performed non-destructively and contactless (long working distance of about 2 cm) with a circular investigated area of 6 mm diameter on the top of samples and without any sampling preparation. The collection and qualitative analysis of acquired data were performed with the OPUS 8.5 spectroscopy software. The reflectance spectra are presented without any spectral correction.

3.4. X-ray fluorescence (XRF) mapping

X-ray fluorescence spectra were acquired by a portable energy-dispersive XRF spectrometer ELIO (Bruker Corporation, Billerica, MA, USA) non-destructively and contactless on polished thin cross-sections. The excitation source works with an Rh anode. XRF measurements were carried out by fixing the tube voltage at 40 kV and the tube current at 80 µA for a measured time of 480 s (8 min) and setting acquisition channels at 2048. The XRF maps (20 rows × 20 columns) were collected with a pixel size of 200 × 100 (horizontal × vertical). The data were processed by ELIO 1.6.0.29 software (Bruker Corporation, Billerica, MA, USA). The polished thin cross sections for the XRF mapping were prepared by embedding a small fragment, sampled from the treated Angera stone, in cold slow-curing epoxy resin (Struers). After 24 h, the samples were cross-sectioned by using a microtome and dry polished with conventional methods (silicon carbide papers with grit from 800 to 2500). A final wet polishing was carried out using in sequence a 6.0 µm and 1.0 µm diamond polishing paste on polishing cloths.

3.5. Scanning electron microscopy (SEM)

Scanning Electron Microscope (SEM) JSM-IT 500 (JEOL, 2019), equipped with an Energy Dispersive Spectrometer (EDS) was used to obtain secondary and backscattered electron (SE and BSE) images at high magnification and rapid semi-quantitative analyses.

3.6. X-ray diffraction computed tomography (XRDCT)

The XRDCT measurements were carried out at the ID15A beamline station of the ESRF (European Synchrotron Radiation facility; Grenoble, France) [33]. The samples were mounted on a sample stage which allowed translational and rotational movements. The energy of the monochromatic pencil beam was tuned to 90 keV (for meteorites and archaeological ceramics) and 42 keV (for the dolostone) using a double-bounce bent Laue monochromator.

The SR X-ray beam was focused down to the micrometer scale (35 µm(h) × 15 µm(v)) using a compound refractive lens transfocator. The investigations were carried out with a state-of-the-art PILATUS3 X CdTE 2 M hybrid photon-counting area detector [20] to record the two-dimensional (2D) diffraction patterns [34].

The XRDCT scans along y were performed over a 180° rotation (ω) and the slice thickness was equal to the vertical beam size (Fig. 1). The sample-to-detector distance and other geometric parameters were calibrated from diffractograms of a capillary sample of NIST SRM674b CeO_2 using PyFAI, a locally modified version of which was also used to azimuthally integrate the projections with outlier rejection to minimise a skewing effect due to the possible presence of large crystallites [35,36].

The exposure time was of about 50–100 ms (depending on the sample) for each projection. 1700 projections were rearranged into sinograms which were subsequently corrected for background scattering. Beamline scripts were then used to perform and interpret tomographic reconstructions of the integrated data [37–39]. With this experimental setup, the measured volume was 1.8 × 1.8 × 1.5 mm^3 and the reconstructed images (tomograms) have a voxel size of 35 × 35 × 15 μm^3. Data collection and XRDCT reconstruction required 8 h per sample.

Regions of interest (ROIs; XRD marker peaks) are selected in the Q space of one-dimensional diffractograms and their signal was plotted as a function of all pixels of the array. The XRDCT reconstruction images are then presented in false colour colourmaps spanning from blue-green (low signal) to red (high integrated area) to show the 3D spatial distribution of specific XRD peaks. Several ROIs over different (*hkl*) reflection peaks of the same crystalline phase were selected to check the reliability of the method.

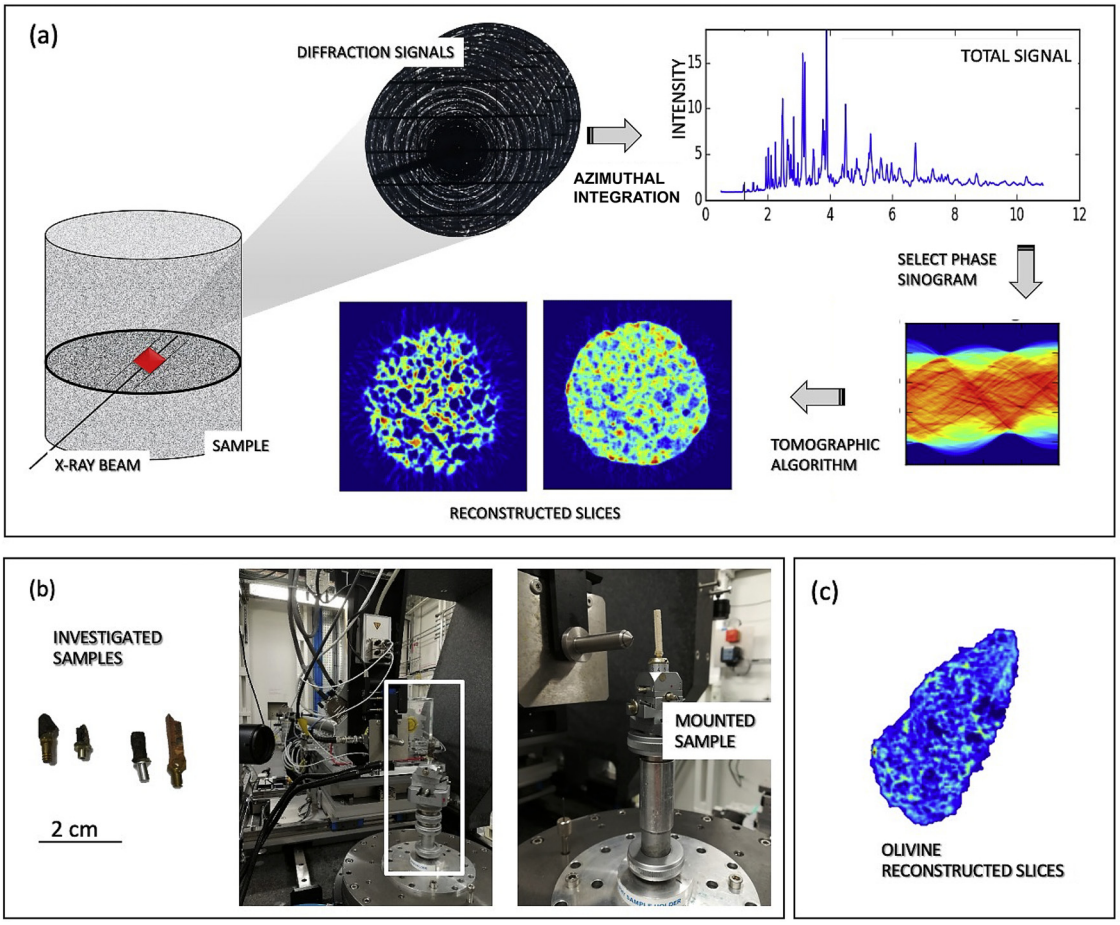

Fig. 1. X-ray diffraction Computed Tomography (XRDCT): (a) reconstruction scheme of the XRDCT analysis; (b) samples investigated in the present study (meteorite, Pietra di Angera, and ancient ceramic) and inset of the experimental setupat ID15B ESRF; (c) example of a reconstructed slice of a *(hkl)* peak mineral phase.

The spatial distribution of selected crystalline phases and possible correlations/ miscorrelations among phases have been explored by comparing different ROI maps. Moreover, RGB colour imaging for retrieving the volume distribution of specific phases has been performed. To do that, the XRDCT image reconstruction in RGB of phases of interest has been split in its red, green, and blue channels, as described in [23]. Then, the red channels of those phases (which represent the regions where the diffraction peak of that crystalline phase has the highest intensity) have been superimposed by using an RGB correlation tool.

The XRD patterns extracted from individual voxels or whole slices of the 3D mineralogical maps were not subjected to any smoothing or post-processing. Note that the diffraction patterns were not corrected for spottiness prior to 1D azimuthal integration. The X'Pert HighScore 2.2.0 software and database (PANalytical) has been used for the qualitative analysis of the XRD datasets. The open-source Fiji software has been used to visualise the XRDCT reconstructed slices [40]. The 3D image renderings have been generated with the commercial software VGStudio 2.0 (Volume Graphics, Germany).

4. Results and discussion

This paragraph will present the results of the CHG characterisation achieved through laboratory and unconventional techniques. Specifically, for each case study, the results obtained at the lab scale (OM, XRD, ER-FTIR; etc.) are presented. Subsequently, the XRDCT outcomes will confirm and/or address questions left unanswered by traditional techniques. Finally, the strengths and limitations of XRDCT in comparison to lab methods will be critically discussed.

4.1. Case study #1: ancient pottery of the Roman age

In sample *ARA13-2*, two different regions (an outer and an inner one) can be well distinguished owing to the colour change of the matrix under the microscope (Fig. 2a).

In its inner part, the very homogeneous matrix is brown in parallel Nicols (N//) and dark brown in crossed Nicols (NX). No crystals are observed within this micromass probably because they are too small to be individually distinguished. Minerals are the most common inclusions: well-rounded grains of quartz with an undulatory extinction effect are poorly sorted and homogeneously dispersed within the matrix and their grain size ranges from fine to medium sand size. A few feldspars with a medium grain size can be detected as inclusions (Fig. 2d). Well-rounded clay-rich inclusions surrounded by ring-voids shrinkage are observed (Fig. 2e). No rock fragments appear as inclusions. Finally, branching elongated voids between crumbs of clays as well as parallel voids resulting from the drying are evident.

The outer portion of the ceramic is easily detectable thanks to the lighter colour of the matrix which can be classified as brown if compared with the inner one (Fig. 2b). Again, this micromass is optically inactive. On the other hand, it has the same mineralogical composition as the inner part of the ceramic even though a smaller grain size and sorting of the mineral inclusions are clear and associated with cracks and voids (Fig. 2c). Here, the quartz inclusions have a grain size moderately bimodal (silt and fine sand size), com-

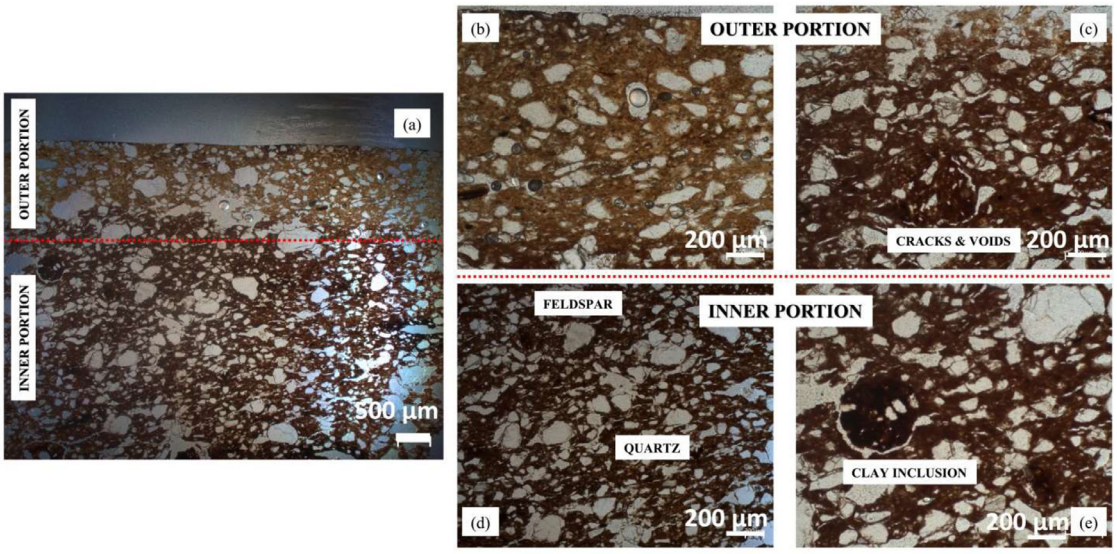

Fig. 2. Optical micrographs of *ARA13-2*: (a) panoramic view of the ancient ceramic where the two different portions can be well distinguished (N//), (b and c) outer portion of the ceramic characterised by mineral inclusions, mainly quartz and feldspar (b), and isooriented cracks and voids (c) (N//); (d and e) inner portion of the ceramic characterised by well-graded mineral (quartz and feldspar) (d) and well rounded clay-rich inclusions (e) (N//).

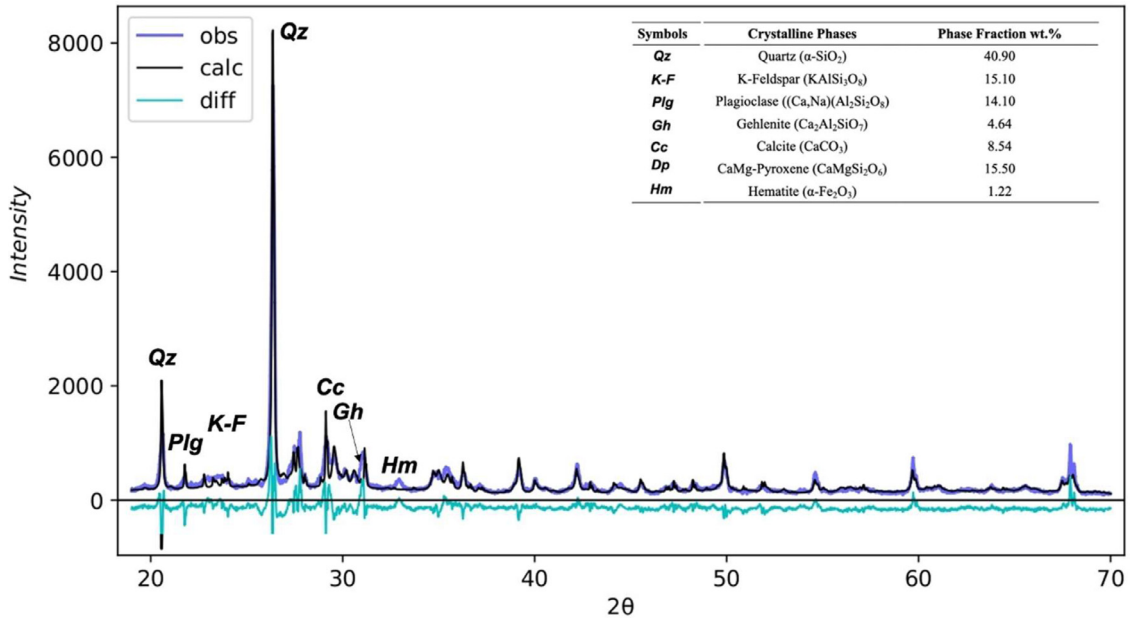

Symbols	Crystalline Phases	Phase Fraction wt.%
Qz	Quartz (α-SiO_2)	40.90
K-F	K-Feldspar ($KAlSi_3O_8$)	15.10
Plg	Plagioclase ($(Ca,Na)(Al_2Si_2O_8)$)	14.10
Gh	Gehlenite ($Ca_2Al_2SiO_7$)	4.64
Cc	Calcite ($CaCO_3$)	8.54
Dp	CaMg-Pyroxene ($CaMgSi_2O_6$)	15.50
Hm	Hematite (α-Fe_2O_3)	1.22

Fig. 3. Rietveld plot of the ancient ceramic. Diffraction peaks of the main phases are labelled. The difference ("diff") between the observed ("obs") and calculated ("calc") profile is not in scale.

posed of rounded and sub-angular inclusions with no preferential alignment.

The XRPD results report that quartz is the most abundant phase associated with K-feldspar. Diffraction peaks attributed to plagioclase, calcite, and Mg-pyroxenes are detected as well as gehlenite and hematite appear as minor phases. In Fig. 3 the XRPD pattern of the ceramic is shown with the main peaks labelled and the quantitative results based on Rietveld analysis are reported.

This complex mineral assemblage (Ca and/or Mg-silicates, Fe oxides, etc.) was not detected during OM probably because these are newly formed phases occurring during firing which is finely dispersed within the matrix.

The distinction between primary minerals (crystal inclusions, i.e. quartz, plagioclase, and K-feldspar), prograde minerals (newly formed phases during firing such as diopside, gehlenite, calcite), and secondary minerals formed during the burial processes of the ceramic lamps using X-ray diffraction analysis (XRD) and OM allowed us to define a rough estimation of the firing temperature. In particular, the occurrence of plagioclase suggests the firing temperature of around 1000 °C, and the presence of CaMg-pyroxene (diopside, $CaMgSi_2O_6$) associated with gehlenite ($Ca_2Al(AlSiO_7)$) allows the assumption that this ceramic was manufactured from carbonate-rich clay raw materials. It is important to stress that the firing process does not necessarily achieve a mineral assemblage that is at thermodynamic equilibrium, and this must be remembered in any attempt to predict the firing properties. Finally, hematite (Fe_2O_3), even if in very low concentration, has been detected in the XRPD patterns, thus suggesting that ceramic manufacture occurred in an oxygen fugacity higher than the hematite-magnetite buffer.

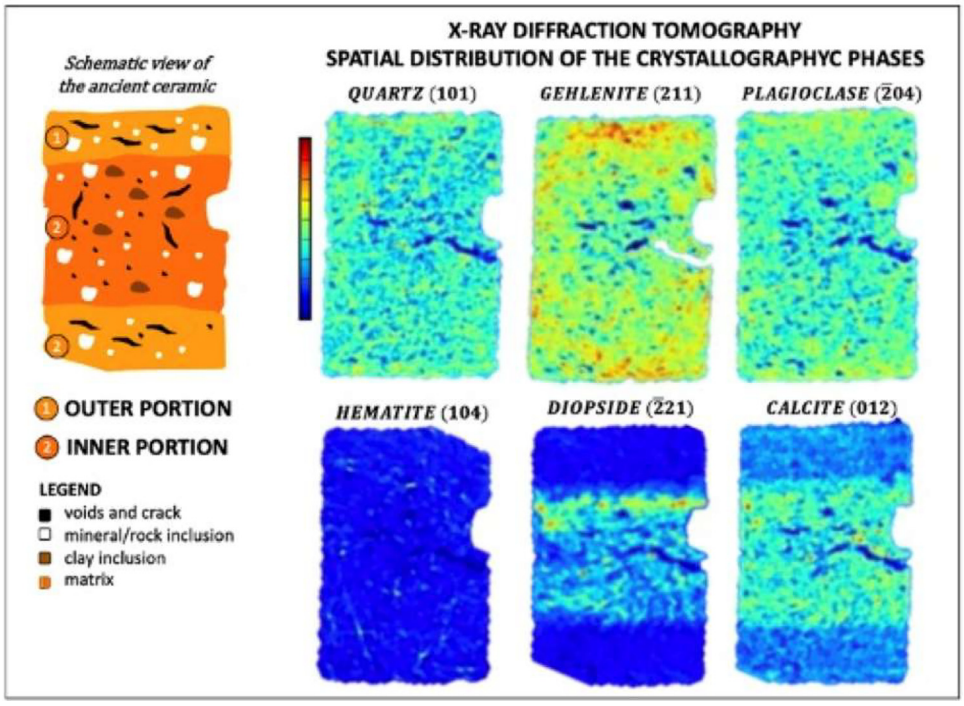

Fig. 4. XRDCT reconstruction images showing the spatial distribution of the main phases within the ancient ceramic. For clarity, a schematic drawing of the ceramic with a clear distinction between the outer and inner portions as observed during OM is also reported (sample size: 2 × 4 mm horizontal x vertical).

The obtained results at the lab scale allow for a comprehensive characterization of the ceramic, yet they still leave some open questions, primarily concerning the ceramic manufacture, i.e., temperature and firing procedures.

In Fig. 4 XRDCT reconstructed slices are shown and the 3D phase distribution of selected phases within the pottery is reported. The colour scale bar given on the left side-hand shows the relative intensity of a (*hkl*) diffraction peak, enabling us to obtain a rough quantitative relative abundance of the phase in the sample. For instance, quartz appears homogeneously dispersed, with a higher concentration in the outer portion.

The XRDCT results identify the same phase assemblage observed during the preliminary analysis at the lab scale but also record their spatial distribution in a completely non-invasive way. It is interesting to note that (i) in the inner portion of the ceramic diopside and calcite coexist whereas (ii) in the outer one gehlenite is associated with plagioclase.

In the inner core, the starting raw materials were probably a mixture of quartz and feldspar grain mixed with a carbonate-rich clay fraction. In this latter, the presence of chlorite and/or vermiculite might have led to the Mg content promoting the crystallisation of the diopside crystals. This area was probably fired at ∼ 1000 °C and the calcite can be interpreted as a reformed (retrograde) phase that has crystallised from the unreacted free lime produced by the thermal decomposition of the original calcite. The incomplete thermal reaction between the free lime with the relicts of clay minerals to form new Ca-silicates might be ascribed to several reasons, such as (*i*) the temperature and/or time insufficient for the occurrence of the complete reaction and (*ii*) an excess amount of calcite concerning the availability of silicate which appears homogeneously dispersed in the whole inner layer (Fig. 4).

In the outer portion of the ceramic, gehlenite associated with plagioclase might attest to a slightly lower firing *T* of the inner part (∼ 900 °C). On the other hand, the clay fraction used in this layer was higher in weight percentage and it was mainly a Si-Al-rich component.

The spatial distribution of these two different phase assemblages suggests that the ceramic manufacture was performed in two different steps: (a) the ceramic body was first fired at high *T*; (b) it was hidden by the overlapping of an engobe, characterised by larger content of the Si-Al rich clay fraction which was fired at a slightly lower *T*.

The homogeneous phase distribution of the hematite within the outer and inner layers confirms that two firing steps all occurred in oxidising conditions.

Finally, from Fig. 4 in the “inner portion” of the ceramic, there is a noticeably higher concentration of the diopside in the outermost layer compared to the inner one. The same applies to the “outer portion” when considering the distribution of gehlenite. This suggests a temperature gradient during the firing process, wherein each layer, the innermost part has reached a lower temperature compared to the outer one.

4.2. Case study #2: revealing the interactions of inorganic conservation treatments with dolomitic stone substrates

The external reflection FTIR (ER-FTIR) spectra collected on the surface of the DAP-treated stone material (Fig. 5a) show the characteristic reflectance bands in the range 3600–3000 (stretching vibrations N–H and/or O–H groups) and in the range 1250–1000 cm^{-1} (stretching vibrations of PO_4 groups) in addition to bands of dolomite of the substrate [41]. These novel reflectance bands can be attributed to hydrated phosphates and demonstrate that the DAP consolidation of the Angera stone promotes the formation of new phosphate phases at the interface between the stone material and the DAP poultice. The DAP reaction with dolomitic grains of the stone matrix can form both Ca-phosphates and Mg-phosphates (CaPs and MgPs respectively [30]). Here, the characteristic reflectance band at 3288 cm^{-1}suggests the crystallisation of an external coating of hydrated magnesium phosphates [41].

On the other hand, considering that ER-FTIR spectroscopy is a surface technique and the instrumental setup used in this study

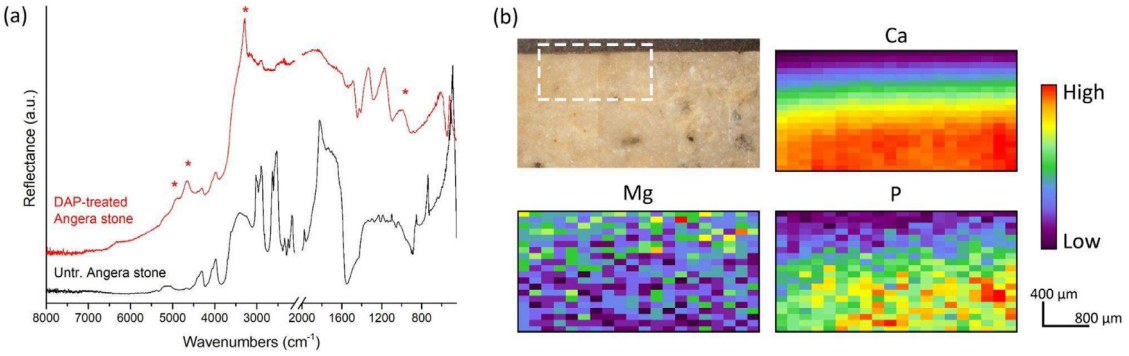

Fig. 5. (a) ER-FTIR spectra collected on the surface of the Angera stone before (black pattern, untreated Angera stone) and after (red pattern, DAP-treated Angera stone) the application of the DAP consolidating poultice. The * symbols point out the reflectance bands attributed to the formation of hydrated phosphates on the treated surface; (b) optical image of the polished cross-section of the DAP-treated Angera stone showing the region (dashed white rectangle) investigated by XRF and micro-XRF maps of calcium (Ca), magnesium (Mg) and phosphorus (P). The black scale bars refer to the size of micro-XRF map.

investigates an area having a 6 mm diameter, the presence of other newly-formed phases (including CaPs) below MgPs and/or in such minor fraction that cannot be detected with this instrumental set up cannot be a priori excluded.

In Fig. 5b the µ-XRF 2D maps collected on polished thin cross sections of the DAP-treatedAngera stone detect phosphorus, attributed to P-containing phases, below the surface and down to ~ 1.5–2 mm (corresponding to the maximum depth investigated in this study). This finding shows evidence of the millimeter diffusion of the DAP solutions within the pore structure of the Angera stone matrix and demonstrates that the DAP interaction with dolomitic stone grains is not confined only to the treated surface or to micrometric subsurface regions of the dolostone. From one side, the investigation of the mutual distribution of newly-formed phases concerning dolomite grains of the stone matrix would provide important information on mechanisms ruling the crystallisation but, due to the elemental nature of the XRF technique, the unambiguous attribution of the P detection in µ-XRF maps to Ca- and/or to Mg-containing phases and/or to a subsurface re-crystallisation of reaction by-products and unreacted reagent is not achievable. On the other side, the spotty localisation of P could be attributed to the particular pore structure of the lithotype and hence to crystallisation phenomena occurring only in correspondence with open and connected voids or cracks, or, on the other side, to the presence of stone regions particularly reactive toward the inorganic treatments (i.e. due to a particular orientation of dolomite crystals within the stone microstructure).

A 3D approach able to identify, (semi-)quantify, and spatially resolve the distribution of P-based compounds and voids would be needed to investigate the crystallisation of P-containing phases within the microcrystalline texture of stone grains and down to the microscale.

The reconstructed XRDCT pattern of an entire representative slice, extracted at about 800 µm from the DAP-treated surface of the Angera stone, is shown in Fig. 6. The XRD pattern of DAP-treated Angera stone is dominated by Bragg peaks of dolomite (Dol). Thanks to the high signal-to-background ratio (inset), the very weak diffraction peaks of struvite (Suv) mixed with minor amounts of clay minerals (Cm) can be detected as well, notwithstanding their intensity is of two to three orders of magnitude below the dolomitic ones. Struvite peaks are detected in the XRD patterns collected either close to the DAP-treated surface or within the stone matrix, and they are observed down to the inner portions of the volume investigated by XRDCT. These results unambiguously confirm the surface identification of struvite hypothesised by ER-FTIR data and, at the same time, demonstrate the crystallisation of this Mg-containing phosphate phase within the treated dolostone. The symmetric and well-resolved diffraction peaks at Q = 1.06 Å^{-1} (d_{010}), 1.12 Å^{-1} (d_{020}), 1.17 Å^{-1} (d_{011}), 1.47 Å^{-1} (d_{111}), and 1.51 Å^{-1} (d_{021}) of struvite prove a quite ordered crystal structure for this newly-formed MgP phase. On the contrary, no Bragg peaks are observed for CaPs in any XRD patterns or XRDCT images of the treated Angera stone. In particular, only a very weak and broad peak at Q 3.67 Å^{-1} (d_{004}) could be attributed to the formation of apatitic phases (i.e. hydroxyapatite, $Ca_5(PO_4)_3(OH)$; amorphous calcium phosphates, $Ca_xH_y(PO_4)_z{\cdot}nH_2O$, with n = 3–4.5 and 15–20 % H_2O) or octacalcium phosphate ($Ca_8(HPO_4)_2(PO_4)_4{\cdot}5H_2O$), but the absence of other characteristic peaks in marker regions or their overlapping with XRD peaks of other phases prevented their unambiguous identification. Most likely, the actual formation of CaPs cannot be excluded but these phases are almost certainly formed in such a poorly crystalline and partially substituted nonstoichiometric form that they cannot be detected even with the high signal-to-background ratio of SR and XRDCT measurements [30].

The spatial distribution of dolomite and struvite phases is displayed with false colours maps in Fig. 6 by subtracting a local linear background and integrating the Bragg peak area in each voxel of the same slice (integrated marker peak at Q = 1.70 Å^{-1} (d_{012}) and at 1.47 Å^{-1} (d_{111}) for dolomite and struvite, respectively). In particular, the XRDCT reconstruction image of dolomite permits to study of the spatial distribution of stone grains within the lithotype as well as to observe the presence of several voids notwithstanding the subsurface crystallisation of phosphate phases. These findings are of remarkable importance in the CH field as the XRDCT datasets indicate that the porosity of the stone materials is preserved after the DAP consolidation of dolostones and demonstrate the capability of inorganic-mineral treatments to not occlude the pore structure of porous stone materials.

The XRDCT data shed new light on the crystal sizes and spatial orientation of newly formed phases. In particular, the XRDCT reconstruction images indicate that struvite consists of thousands of 3D randomly oriented crystallites within the dolostone, as demonstrated by the absence of single crystal spots and/or artefacts. As for the crystallisation mechanism of reaction products, the RGB colour imaging of Fig. 6d permits a step further in its understanding. By graphically overlapping the regions where the two phases are more abundant (highlighted by the spatial distribution of red channels of XRDCT images fraction, as described in §3.6 of the Methods section), it is possible to semi-quantitatively study the mutual localisation of dolomite and struvite in a certain volume. Here, the partial superimposition of struvite and dolomite shows the nucleation and growth of newly formed crystals from stone grains of the stone matrix (regions of co-existence, yellow in

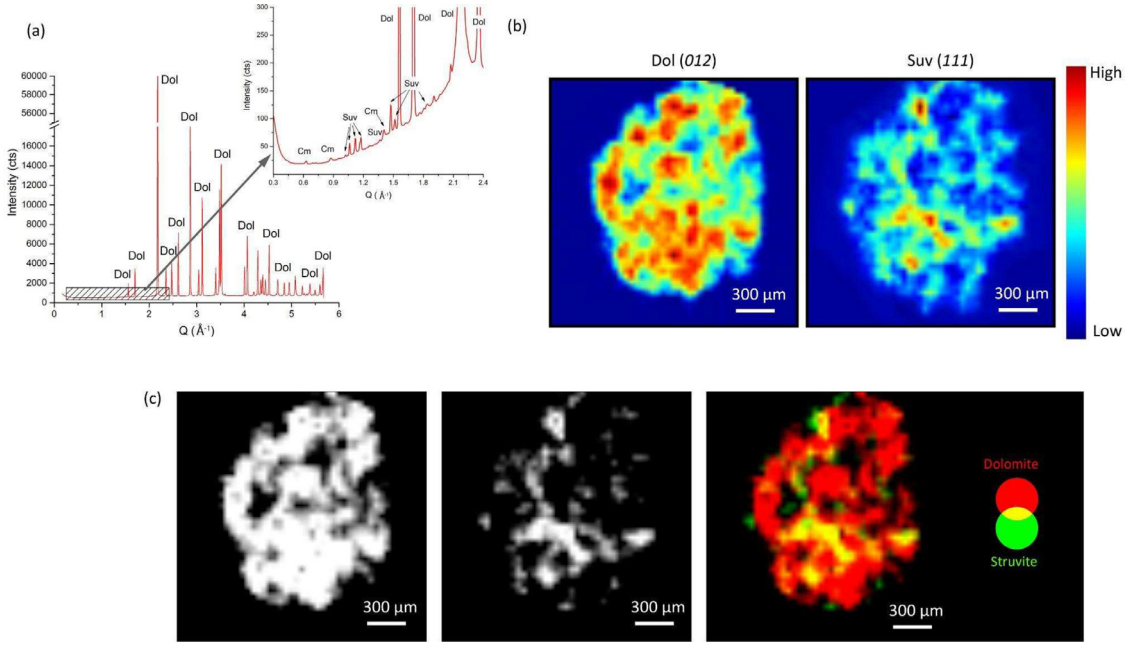

Fig. 6. (a) Sum of XRD pattern of the DAP-treated Angera stone extracted from a representative slice of XRDCT datasets. The XRD pattern is dominated by Bragg peaks of dolomite (Dol). The inset, showing detail in the 0.3–2.4 Å^{-1} Q-range of the XRD pattern, highlights the presence of accessory clay minerals (Cm) of the original stone matrix and newly-formed struvite (Suv); (b) XRDCT reconstruction images obtained by integrating the XRD marker peaks in the Q-range 1.68–1.72 Å^{-1} (max at Q 1.70 Å^{-1} (d_{012}) and 1.45–1.49 Å^{-1} (max at Q 1.47 Å^{-1} (d_{111}) of the spatial distribution of dolomite (Dol) and struvite (Suv), respectively; (c) Red channels of XRDCT image reconstruction (obtained as described in §3.6 of the Methods section and in [23]) of dolomite (left) and struvite (middle), and their RGB merged imaging (right). The XRD pattern and the XRDCT image reconstructions of this figure are extracted at about 800 µm from the treated surface of the Angera stone.

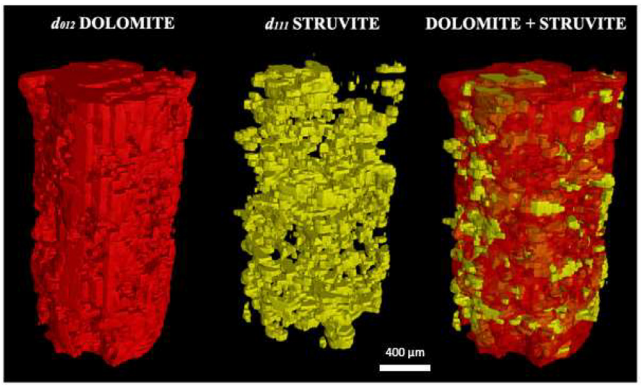

Fig. 7. 3D spatial distribution extracted from XRDCT results of dolomite and struvite in the DAP-treated Angera stone obtained by plotting the red channel of the RGB images. In the volume rendering on the right, the orange colour shows the overlapping regions of dolomite and struvite.(For interpretation of the references to color in this figure legend, the reader is referred to the web version of this article.)

Fig. 6d). Moreover, the RGB correlations point out the crystalline network formed by struvite crystallites that can connect detached dolomite grains. This consolidating action can be further appreciated in the volume renderings of the XRDCT datasets shown in Fig. 7 which demonstrate the remarkable binding effect carried out by the MgPs network down to the inner portions of the investigated volume of DAP-treated Angera stone.

Here, the significant step forward concerning literature data is the opportunity to study the partial dolomite-to-magnesium phosphate conversion occurring during DAP treatments non-destructively, with microscale 3D spatial resolution. These results strongly improve knowledge of inorganic-mineral treatments by both assessing the variations induced by DAP consolidating solution to the original dolostone in terms of newly-formed phase composition and their 3D spatial distribution and understanding the influence of these features on the crystallisation of the new phases formed by the conservation treatment.

4.3. Case study #3: meteorite

The Mineralogical Collection Museum houses a 10 cm diameter sample of the Holbrook meteorite, along with smaller centimetre-sized samples that are likely from the same meteorite but remain unidentified. This has provided the opportunity for both conventional analyses, including thin section, microprobe analysis, and diffraction, as well as non-conventional analysis utilizing XRDCT to assess the sample's mineralogical composition in a non-destructive manner.

Holbrook belongs to the L/LL chondrite geochemical group, which has intermediate iron abundance between low-Fe L chondrites and very low-Fe LL chondrites [32]. Only eleven L/LL meteorites with witnessed impacts have been recovered, and Holbrook is one of the four whose fall was witnessed, classified precisely as an L/LL6 ordinary chondrite in the Meteoritical Bulletin Database. Many fragments of the Holbrook meteorite have been recovered since its fall, and as several of these fragments were altered, they allowed for the study of surface alteration rates on Earth (Fig. 8a).

The meteorite contains chondrules, ranging in size from 0.5 to 1.5 mm in diameter, and is mainly composed of olivine and low-calcium orthopyroxene. Microprobe analysis and laboratory microdiffraction have confirmed the presence of these components (olivine Fo75 and orthopyroxene En68) along with albitic plagioclase rims (Fig. 8b). The chondrules are surrounded by a fine recrystallized matrix, rich in olivine and pyroxenes, along with aggregates of iron-nickel alloys and troilite (Fig. 8c). These aggregates are dispersed throughout the matrix and are also found along the edges of the chondrules.

The mineralogical composition and spatial distribution of the constituents of the analyzed meteorite fragment was identified using non-invasive XRDCT. The presence of olivine, pyroxene, iron-nickel alloy, and troilite was verified, which are all phases compat-

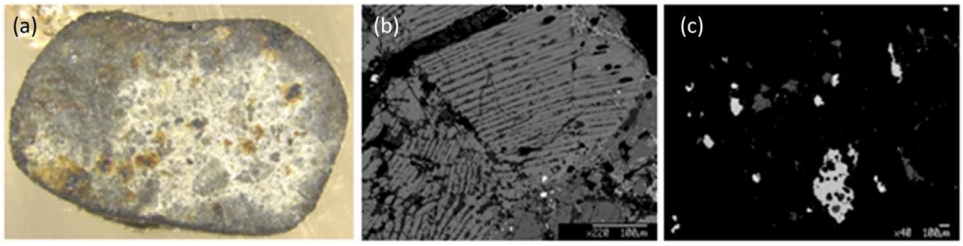

Fig. 8. (a) Polished section image showing chondrules, matrix, silicate crystals, metal and sulfides, and alteration of metallic fragments. (b) SEM image of a chondrule with olivine (Fo75) and orthopyroxene (En68) components and albitic plagioclase rims. (c) SEM image of iron/nickel alloy and troilite aggregates in the matrix.

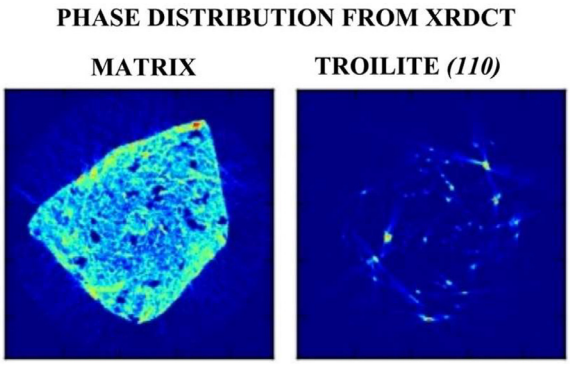

Fig. 9. XRDCT reconstruction images showing the spatial distribution of the main phases within the meteorite.

ible with the composition of the Holbrook meteorite [32]. In Fig. 9 it is clear that the silicates and iron-nickel alloy constitute a very dense and micrometric "matrix" where large and single crystals of troilite appear. Image analysis was applied to selected sections reconstructed based on the diffraction peaks of the main phases, revealing both textural features and the volume fraction of each phase (Fig. 9). The combination of olivine and pyroxene makes up 81 % of the volume, followed by the iron-nickel alloy at 10 %, and troilite and other minor phases at 9 %.

The results of both partially destructive conventional analyses and non-invasive XRDCT analyses have confirmed that the mineralogy of the two fragments analysed is compatible with the mineralogy of the Holbrook meteorite, allowing for the identification and the possibility of using these fragments instead of the large museum sample for further scientific investigations. Furthermore, it has been demonstrated that non-invasive XRDCT analyses accurately allow for both overall mineralogical determination using diffraction information and modal and spatial analysis using image analysis. These findings suggest that non-invasive XRDCT methods have promising applications for future mineralogical studies of meteorites.

Conclusions: a new perspective in the characterisation of Cultural Heritage Geomaterials (CHG). An overview of XRDCT **progress/potentials and limits.**

The unique information provided from XRDCT experiments advances knowledge on CH systems non-invasively and holds significant potential for understanding the properties. and performance of other geomaterials in the Cultural Heritage field. Consequently, XRDCT shows great promise to be a complementary tool to existing imaging techniques, allowing the structural analysis and real volume distribution of crystalline/amorphous phases, unlike 2D techniques where volume information is not available.

The potential of XRDCT as a non-destructive and/or non-invasive structural tool to explore the crystallo-chemical composition, topography, and textural features of geomaterials has been explored. As demonstrated, XRDCT enables to collect 3D datasets on different typologies of heterogeneous geomaterials, combining qualitative analysis based on diffraction data with tomographic volume reconstructions (2D distribution maps, virtual cross sections, and 3D (volumes) of crystalline phases).The XRDCT experimental setup does not require sample preparation and therefore preserves the original textural and microstructural features of the specimens, which can be reused for further investigations. It has a strong relevance when dealing with Cultural Heritage micro-samples or objects where the need to obtain the maximum amount of information meets the need to develop non-destructive and non-invasive analytical techniques. Additionally, it enables the characterization of even very small-sized samples. Further studies can facilitate the extrapolation of the crystal orientation within the samples; a parameter of paramount importance, especially in the study of alloys.

Virtual cross-sections of selected phases can be computed and isolated from an unknown bulk sample without requiring *priori* knowledge of its composition, texture, or phase orientation.

Overall, ongoing efforts in software development and computational methodologies aim to enhance the robustness and applicability of XRDCT, overcoming its inherent limitations and expanding its utility in materials science and related fields.

The limitations of XRDCT include the possible presence of artefacts rising from large crystallites, which leads to single-crystal XRD patterns and not to powder-like rings, or very small crystallites leading to the loss of Bragg diffraction signals.

Moreover, the availability of commercial software to manage complex and large XRDCT datasets is limited. Consequently, researchers often rely on ad hoc algorithms, newly developed software, and advanced computing tools to address these challenges advanced computing tools. For instance, filtering procedures and data management are devised to mitigate artifacts arising from large crystallites. Additionally, advancements such as pair distribution function computed tomography for the latter are being pursued to tackle the issue of Bragg diffraction loss associated with very small crystallites.

Although the samples do not necessitate specific preparation (e.g., embedding in resin, polishing), the nature of the sample and its size need to be carefully selected to achieve the best "compromise" among the desired voxel resolution (the smaller the beam size, the smaller the voxel size; the samples should be small enough to achieve the highest voxel size resolution but big enough to be representative of the investigated system), the acquisition time (the smaller the voxel size, the longer the acquisition time) and the "ideal powder assumption" (decreasing the beam size decreases the maximum average crystallite size that satisfy the assumption).

The SR beam energy can be tuned in the experimental hutch depending on the nature of the sample, as showed in this study. However, it should be considered that some compounds or crystalline phases may not be stable to the high X-ray flux and thus

decay or transform into other phases during the investigations if care is not taken to tune beam parameters to avoid this. On the other side, SR facilities allow to set of several experimental parameters at the XRDCT beamlines, which permits to study of beam-sensitive samples/objects without (or with the minimum) beam damages.

The next steps of this research will integrate micro-CT and XRDCT investigations on the same sample, facilitating a multimodal tomography analysis. This approach will enable a comprehensive understanding of the sample's structure and composition.

Data availability

The raw/processed data required to reproduce these findings cannot be shared at this time due to technical or time limitations. They will be shared on request.

CRediT authorship contribution statement

Elena Possenti: Supervision, Formal analysis, Data curation, Conceptualization, Investigation, Methodology, Writing – original draft, Writing – review & editing. **Maria Catrambone:** Data curation. **Chiara Colombo:** Formal analysis, Writing – original draft. **Marco Cantaluppi:** Formal analysis. **Marco Merlini:** Formal analysis, Writing – original draft. **Gavin B.M. Vaughan:** Methodology, Software. **Marco di Michiel:** Methodology, Software. **Nicoletta Marinoni:** Supervision, Formal analysis, Data curation, Conceptualization, Investigation, Methodology, Writing – original draft, Writing – review & editing.

Acknowledgments

The authors gratefully acknowledge the European Synchrotron Radiation Facility E.S.R.F. and the ID15A beamline for the allocation of experimental beamtime (proposal HG-131 (2018): "X-ray diffraction microtomography of inorganic consolidants applied to carbonatic stones of historical monuments"). The authors acknowledge the support of the Italian Ministry of Education (MUR) through the project "Dipartimenti di Eccellenza 2023–2027". We also acknowledge Dr Laura Leone for contributing to data data acquisition and data processing during her MSc research thesis.

References

[1] D. Comelli, G. Mac Lennan, M. Ghirardello, A. Phenix, Anal. Chem. 91 (2019) 3421–3428, doi:10.1021/acs.analchem.8b04914.
[2] M. Segata, N. Marinoni, M. Galimberti, M. Marchi, M. Cantaluppi, A. Pavese, A.G. De la Torre. Angeles, Mater. Charact. 155 (2019) 109809, doi:10.1016/j.matchar.2019.109809.
[3] E. Possenti, C. Conti, C. Colombo, L. Gigli, M. Merlini, J.R. Plaisier, M. Realini, G.D. Gatta, Analysts 143 (2018) 4290–4297, doi:10.1039/C8AN00901.
[4] E. Possenti, C. Conti, C. Colombo, L. Gigli, M. Merlini, J.R. Plaisier, M. Realini, G.D. Gatta, Appl. Phys. A 124 (2008) 383, doi:10.1007/s00339-018-1798-8.
[5] J.L. Perez-Rodriguez, M. del C. Jimenez de Haro, B. Siguenza, K.M. Martinez-Blanes, Appl. Clay Sci. 116-117 (2015) 211–219, doi:10.1016/j.clay.2015.03.016.
[6] M.V. Cotte, V. Gonzalez, F. Vanmeert, et al., Molecules 27 (6) (2022), doi:10.3390/molecules27061997.
[7] M. Ghirardello, M. Gonzalez, L. Monico, A. Nevin, D. Mac Lennan, et al., Microsc. Microanal. 28 (2022) 1504–1513, doi:10.1017/S1431927622000873.
[8] G. Massinelli, N. Marinoni, C. Colombo, G.D. Gatta, M. Realini, M. Burghammer, E. Possenti, Sci. Rep. 14 (2024) 9108, doi:10.1038/s41598-024-58718-z.
[9] G. Gonzalez, G. Wallez, T. Calligaro, M. Cotte, W. de Nolf, et al., Anal. Chem. 89 (2017) 13203–13211, doi:10.1021/acs.analchem.7b02949.
[10] E. Possenti, C. Colombo, C. Conti, N. Marinoni, M. Merlini, R. Negrotti, M. Realini, G.D. Gatta, Mater. Charact. 154 (2019) 315–324, doi:10.1016/j.matchar.2019.05.037.
[11] M. Cantaluppi, N. Marinoni, F. Cella, F. Camara, G. Borghini, W. Kagan, Cem. Concr. Res. 148 (2021) 106533, doi:10.1016/j.cemconres.2021.106533.
[12] V. Caruso, N. Marinoni, V. Diella, F. Berna, M. Cantaluppi, L. Mancini, L. Trombino, C. Cattaneo, L. Pastero, A. Pavese, Archaeol. Anthropol. Sci. 12 (2020) 162, doi:10.1007/s12520-020-01090-6.
[13] N. Marinoni, M. Voltolini, L. Mancini, F. Cella, J. Mater. Sci 47 (2012) 2845–2855, doi:10.1007/s10853-011-6114.
[14] N. Marinoni, M. Voltolini, M.A.T.M. Broekmanns, L. Mancini, P.J. Monteiro, N. Rotiroti, E. Ferrari, A. Bernasconi A, J. Mater. Sci 50 (2015) 7985–7997, doi:10.1007/s10853-015-9364-7.
[15] P. Bleuet, E. Welcomme, E. Dooryhée, J. Susini, J.L. Hodeau, Nat. Mater. 7 (2008) 468–472, doi:10.1038/nmat2168.
[16] G. Massinelli, E. Possenti, C. Colombo, G.D. Gatta, M. Realini, N. Marinoni, Constr. Build. Mater. 397 (2023) 13234, doi:10.1016/j.conbuildmat.2023.132348.
[17] G. Artioli, T. Cerulli, G. Cruciani, M.C. Dalconi, G. Ferrari, M. Parisatto, A. Rack, R. Tucoulou, Anal. Bioanal. Chem. 397 (2010) 2131–2136, doi:10.1007/s00216-010-3649-0.
[18] M. Voltolini, M.C. Dalconi, G. Artioli, M. Parisatto, L. Valentini, V. Russo, J. Appl. Crystallogr. 46 (2013) 142–145, doi:10.1107/S0021889812046985.
[19] A. Vamvakeros, S.D.M. Jacques, M. Di Michiel, V. Middelkoop, C.K. Egan, R.J. Cernik, A.M. Beale, J. Appl. Crystallogr. 48 (2015) 1943–1955, doi:10.1107/S1600576715020701.
[20] A. Vamvakeros, S.D.M. Jacques, V. Middelkoop, M. Di Michiel, C.K. Egan, I.Z. Ismagilov, G.B.M. Vaughan, F. Gallucci, M. Van Sint Annaland, P.R. Shearing, R.J. Cernik, A.M. Beale, Chem. Commun. 51 (2015) 12752–12757, doi:10.1039/C5CC03208.
[21] W. De Nolf, F. Vanmeert, K. Janssens, J. Appl. Crystallogr. 47 (2014) 1110–1117, doi:10.1107/S1600576714008218.
[22] F. Vanmeert, G. Vandersnickt, K. Janssens, Angew. Chemie - Int. Ed. (2015), doi:10.1002/anie.201411691.
[23] E. Possenti, C. Conti, G.D. Gatta, N. Marinoni, M. Merlini, M. Realini, G.B.M. Vaughan, C. Colombo, Iscience, 25 (2022) 105112, doi:10.1016/j.isci.2022.105112.
[24] Bordet, J. Anal. At. Spectrom. 36 (1724) 202.
[25] Autran, Anal. Chem. 93 (2021) 1135.
[26] E. Possenti, N. Marinoni, C. Conti, M. Realini, G.B.M. Vaughan, C. Colombo, Analyst 149 (2024) 2059–2072, doi:10.1039/D3AN02208K.
[27] D. Gullotta, M. Bertoldi, S. Bortolotto, P. Fermo, A. Pizzalunga, L. Toniolo, Environ. Earth Sci. 69 (2013) 1085–1094, doi:10.1007/s12665-012-2165-2.
[28] A. Cavallo, A.C. Bigioggero, A. Tunisi, Period. Miner. 73 (2004) 197–210.
[29] C. Colombo, C. Conti, M. Realini, A. Sansonetti, Proc. Int. Conf. Heritage, Weather. Conserv. HWC, 2006
[30] E. Possenti, C. Colombo, C. Conti, L. Gigli, M. Merlini, J.R. Plaisier, M. Realini, D. Sali, G.D. Gatta, Constr. Build. Mater. 195 (2019) 557–563, doi:10.1016/j.conbuildmat.2018.11.07.
[31] E. Possenti, C. Conti, G.D. Gatta, M. Realini, C. Colombo, Coatings 9 (2019) 169, doi:10.3390/coatings9030169.
[32] B. Mason, H.B. Wiik, Geochim. Cosmochim. Acta 3-4 (1961) 267–283, doi:10.1016/S0016-7037(61)80062-8.
[33] G.B.M. Vaughan, R. Baker, R. Barret, J. Bonnefoy, T. Buslaps, S. Checchia, D. Duran, F. Fihman, P. Got, J. Kieffer, S.A.J. Kimber, K. Martel, C. Morawe, et al., J. Synchrotron Radiat. 27 (2020) 515–528, doi:10.1107/S1600577519016813.
[34] A. Vamvakeros, S.D.M. Jacques, M. Di Michiel, P. Senecal, V. Middelkoop, R.J. Cernik, A.M. Beale, J. Appl. Crystallogr. 49 (2016) 485–496, doi:10.1107/S160057671600131X.
[35] G. Ashiotis, A. Deschildre, Z. Nawaz, J.P. Wright, D. Karkoulis, F.E. Picca, J. Kieffer, J. Appl. Crystallogr. 48 (2015) 510–519, doi:10.1107/S1600576715004306.
[36] J. Kieffer, J.P. Wright, Powder Diffr. 28 (2013) 339–350, doi:10.1017/S0885715613000924.
[37] S.D.M. Jacques, M. Di Michiel, S.A.J. Kimber, X. Yang, R.J. Cernik, A.M. Beale, S.J.L. Billinge, Nat. Commun. 4 (2013) 2536–2572.
[38] S.D.M. Jacques, M. Di Michiel, A.M. Beale, T. Sochi, M.G. O'Brien, L. Espinosa-Alonso, B.M. Weckhuysen, P. Barnes, Angew. Chem., Int. Ed. 50 (2011) 10148–10152.
[39] M.G. O'Brien, S.D.M. Jacques, M. Di Michiel, P. Barnes, B.M. Weckhuysen, A.M. Beale, Chem. Sci. 3 (2012) 509–523.
[40] J. Schindelin, I. Arganda-Carreras, E. Frise, V. Kaynig, M. Longair, T. Pietzsch, A. Cardona, Nat. Methods 9 (2012) 676–682, doi:10.1038/nmeth.2019.
[41] B. Bindhu, T.A. Thambi, Int. J. Sci. Res. Publ. 2 (2012) 1–4.